Retrieval of Semitransparent Ice Cloud Optical Thickness From Atmospheric Infrared Sounder (AIRS) Measurements

Heli Wei, Ping Yang, Jun Li, Bryan A. Baum, Hung-Lung Huang, Steven Platnick, Yongxiang Hu, and Larrabee Strow

***Abstract*—An approach is developed to infer the optical thickness of semitransparent ice clouds (when optical thickness is less than 5) from Atmospheric Infrared Sounder (AIRS) high spectral resolution radiances. A fast cloud radiance model is developed and coupled with an AIRS clear-sky radiative transfer model for simulating AIRS radiances when ice clouds are present. Compared with more accurate calculations based on the discrete ordinates radiative transfer model, the accuracy of the fast cloud radiance model is within 0.5 K (root mean square) in terms of brightness temperature (BT) and runs three orders of magnitude faster. We investigate the sensitivity of AIRS spectral BTs and brightness temperature difference (BTD) values between pairs of wavenumbers to the cloud optical thickness. The spectral BTs for the atmospheric window channels within the region 1070–1135 cm^{-1} are sensitive to the ice cloud optical thickness, as is the BTD between 900.562 cm^{-1} (located in an atmospheric window) and 1558.692 cm^{-1} (located in a strong water vapor absorption band). Similarly, the BTD between a moderate absorption channel (1587.495 cm^{-1}) and the strong water absorption channel (1558.692 cm^{-1}) is sensitive to ice cloud optical thickness. Neither of the aforementioned BTDs is sensitive to the effective particle size. Thus, the optical thickness of semitransparent ice clouds can be retrieved reliably. We have developed a spectrum-based approach and a BTD-based method to retrieve the optical thickness of semitransparent ice clouds. The present retrieval methods are applied to a granule of AIRS data. The ice cloud optical thicknesses derived from the AIRS measurements are compared with those retrieved from the Moderate Resolution Imaging Spectroradiometer (MODIS) 1.38- and 0.645-μm bands. The optical thicknesses inferred from the MODIS measurements are collocated and degraded to the AIRS spatial resolution. Results from the MODIS and AIRS retrievals are in reasonable agreement over a wide range of optical thicknesses.**

***Index Terms*—Atmospheric Infrared Sounder (AIRS), ice clouds, infrared radiation transfer, optical thickness, retrieval.**

Manuscript received February 9, 2004; revised June 16, 2004. This work was supported in part by the GIFTS-IOMI MURI Project, in part by the National Science Foundation Physical Meteorology Program (managed by Dr. W. A. Cooper) under CAREER Award Grant ATM-0239605, in part by the National Aeronautics and Space Administration Radiation Science Program (managed by Dr. H. Maring, previously by Dr. D. Anderson) under Research Grant NAG-1-02002, and in part by the National Oceanic and Atmospheric Administration under ABI/HES Program NA07 EC00676.

H. Wei and P. Yang are with the Department of Atmospheric Sciences, Texas A&M University, College Station, TX, 77843 USA (e-mail: pyang@ariel.met.tamu.edu).

J. Li and H.-L. Huang are with Cooperative Institute for Meteorological Satellite Studies, University of Wisconsin-Madison, Madison, WI 53706 USA.

B. A. Baum and Y. Hu are with NASA Langley Research Center, Hampton, VA 23681 USA.

S. Platnick is with the NASA Goddard Space Flight Center, Greenbelt, MD 20771 USA.

L. Strow is with the Physics Department, University of Maryland Baltimore County, Baltimore, MD 21250 USA.

Digital Object Identifier 10.1109/TGRS.2004.833780

I. Introduction

ICE CLOUDS cover a substantial portion of the globe [1] and are important to understanding the earth's energy budget and climate [2]–[4]. Because of the difficulty in detecting and analyzing optically thin ice clouds in satellite imager data, more uncertainties remain for ice clouds than for water clouds. *In situ* measurements of cirrus are relatively scarce because these clouds are located at high altitudes, and accurate detection and analysis are problematic. An approach based on the visible and near-infrared (IR) spectral signatures, originally developed by Nakajima and King [5], has been used to infer cloud properties (in particular, effective particle size and optical thickness) acquired from the Moderate Resolution Imaging Spectroradiometer (MODIS) on the National Aeronautics and Space Administration (NASA) Earth Observing System (EOS) Terra and Aqua platforms, as described by King *et al.* [6] and Planick *et al.* [7]. Other algorithms developed by Ou *et al.* [8], [9] and Minnis *et al.* [10], [11] have been applied to different satellite sensors such as the Advanced Very High Resolution Radiometer (AVHRR). Baran *et al.* [12] and Doutriaux-Boucher *et al.* [13] used Along Track Scanning Radiometer 2 (ASTR-2) and Polarization and Directionality of the Earth's Reflectances (POLDER) data, respectively; these instruments provide dual or multiple-viewing of a target. Recently, the MODIS 0.645- and 1.38-μm bands have been used to derive ice cloud reflectance and optical thickness [14], [15]. Such approaches, however, are limited to daytime application because solar illumination is necessary.

To derive ice cloud properties using an alternative methodology that is independent of solar illumination, the IR split window technique [16]–[18] has been developed on the basis of the different absorption properties of ice at the two wavelengths of 11 and 12 μm. High spectral resolution IR radiation measurements have been available from aircraft platforms and are now available from spaceborne platforms. As part of EOS, the Atmospheric Infrared Sounder (AIRS) [19] is designed to provide profiles of atmospheric temperature, moisture, and other gases with high accuracy. The spatial resolution of AIRS is 13.5 km at nadir. Most of the observed AIRS fields of view (FOVs) are not cloud free, and the upwelling IR radiances are modulated strongly by ice clouds. The radiances contaminated by clouds are more problematic for sounding retrievals, requiring the use of cloud-clearing techniques [20]. The AIRS has 2378 IR channels, measuring radiances within 649.5–1136.5 cm^{-1} (15.40–8.80 μm), 1216.5–1613.7 cm^{-1}

(8.22–6.20 μm), and 2181.3–2665.0 cm^{-1} (4.58–3.74 μm), with a spectral resolution of $\nu/\Delta\nu = 1200$, where ν is the wavenumber, and $\Delta\nu$ is the width of the band. Recent studies have shown that the high spectral resolution radiances contain important information on high-altitude ice clouds [21]–[23]. Recently, DeSousa-Machado *et al.* [24] performed global retrievals of cloud properties using the AIRS measured radiances. Kahn *et al.* [25] investigated the infrared spectral feature of very small cirrus particles using the AIRS measurements. Huang *et al.* [26] studied the information content of very high-resolution IR spectra to study thin cirrus clouds.

This study is intended to explore a methodology for retrieving ice cloud optical thickness from AIRS radiances. A fast cloud radiance model is developed to provide the forward simulations when ice clouds are present. Sensitivity studies are carried out to investigate the relationship between the IR spectral brightness temperatures (BTs) and the brightness temperature difference (BTD) between pairs of channels to the optical properties of ice clouds. Based on the sensitivity study, an algorithm is developed for inferring the optical thickness of semitransparent ice clouds. The AIRS-based retrieval results are compared with those derived from the MODIS 1.38- and 0.645-μm bands that have been collocated and spatially degraded to match the AIRS FOVs.

This paper is organized as follows. Section II discusses the fast radiative transfer model for cloudy conditions. The sensitivity studies and the retrieval algorithm for deriving ice cloud optical thickness are presented in Sections III and IV. A case study is presented in Section V. A brief discussion and summary are given in Section VI.

II. Fast Cloud Radiative Transfer Model

Although an existing radiative transfer model, such as the line-by-line atmospheric molecular optical thickness computation [27], can be combined with the discrete ordinates radiative transfer (DISORT) [28] method to simulate cloud high-resolution IR spectral radiances, the computational requirements are quite demanding. A fast, yet accurate, model for simulating high spectral resolution cloud radiances would be quite useful for AIRS analyses. Strow *et al.* [29], [30] developed a fast model to simulate clear-sky AIRS radiances. The fast model uses realistic profiles to produce the transmittance coefficients for atmospheric gas constituents within an atmosphere modeled as having a discrete number of vertical layers. The effective layer transmittances for a given profile are computed quickly by calculating the appropriate predictor values for the profile and multiplying them by the coefficients. Fishbein *et al.* [31] simulated AIRS radiances by adding a random variable cloud amount. Our approach to the development of a fast cloud radiative transfer model is presented in the following section.

A. Single-Scattering Properties of Ice Clouds

Ice clouds are composed of ice crystals with complex nonspherical shapes. The importance of using more realistic ice crystal scattering models in satellite imager-based retrievals has been demonstrated by Mishchenko *et al.* [32]. Heymsfield and Iaquinta [33] showed that in the upper portions of cirrus clouds, the ice particles tend to be quite small, with aspect ratios (i.e., the ratio of particle length to its width) close to unity. Yang *et al.* [34] suggested that the shape of these small ice crystals may be represented by the droxtal geometry. *In situ* measurements from the First International Satellite Cloud Climatology Project Regional Experiment-II (FIRE-II) held in Coffeyville, KS, in 1991, have shown that the middle layers of midlatitude synoptical-scale cirrus clouds are often composed of pristine particles such as hexagonal columns (see [33, Fig. 15]). In the lower portions of cirrus clouds, the ice particles tend to be larger and composed of irregular aggregates. Based on these observations, we assume a general habit distribution for ice clouds: droxtals for small particles (0–50 μm), pristine hexagonal columns for moderately sized particles (50–300 μm), and aggregates for large particles (> 300 μm).

There are numerous methods for computing the single-scattering properties of nonspherical ice crystal particles (see [35] and references cited therein), but no one method is applicable to calculate the single-scattering properties of ice crystals with a variety of shapes and sizes. In the present study, the scattering efficiencies, absorption efficiencies, and asymmetry factors of droxtals, pristine hexagonal columns, and aggregates are computed using the finite-difference time-domain (FDTD) method [36], [37] for small particles. A composite method originally developed by Fu *et al.* [38], [39] is used to derive the extinction efficiencies, absorption efficiencies, and asymmetry factor for moderate to large particles from a combination of an improved geometric optics method (IGOM) [40] and an equivalent sphere approximation. The technical details of this approach can be found in [38], [39], and [41].

Ice particle extinction efficiency, absorption efficiency, and asymmetry factor are shown in Fig. 1 as functions of the particle maximum dimension (left panel) and effective particle size (right panel) for randomly oriented droxtals, pristine hexagonal columns, and aggregates. The effective diameter or effective particle size of a crystal is defined as the ratio of its volume to its projected area and multiplied by 1.5. The aspect ratio and geometry of hexagonal columns are defined by Yang *et al.* [41]. The geometries of the droxtal and aggregate are defined by Zhang *et al.* [42] and Yang and Liou [43], respectively. We compute the single-scattering properties in 76 size bins ranging from 1–10 000 μm (in maximum dimension) for hexagonal columns, 36 size bins from 1–10 000 μm for aggregates, and 28 size bins from 1–1000 μm for droxtals.

The extinction efficiencies have several maxima due to the phase interference of waves through the particles. The positions and amplitudes of maxima are different for each crystal habit. The first maximum in the extinction efficiency occurs at maximum dimensions of 14.3, 18.1, and 55.9 μm for the hexagonal column, droxtal, and aggregate, respectively. For small particles having aspect ratios close to unity, the hexagonal column has the largest volume and effective diameter because the maximum dimension of a hexagon column is defined as its length, while the aggregate has smallest volume and effective diameter. Note, however, that the use of the aggregate shape may not be very realistic for the simulation of very small crystals. The first peak of the extinction efficiency occurs at a smaller particle dimension

for hexagonal crystals than for droxtals and aggregates. Additionally, the first peak of the extinction efficiency for droxtals falls between those for the hexagonal column and the aggregate. When the maximum dimension of an ice crystal is larger than 500 μm, the extinction efficiencies for the three ice habits converge to 2, the asymptotic limit of the geometric optics solution. The optical properties as functions of effective size are provided on the right panel of Fig. 1. The differences are smaller relative to the left panel, particularly for small particle sizes. The main point is that the scattering properties of ice crystals are different over a wide range of particle sizes.

The comparisons of absorption efficiencies and asymmetry factors for the three habits are quite similar to the case for the extinction efficiency. Although the patterns of these curves for three ice crystal habits are similar, the amplitudes or the positions of the maxima for each habit are different. When the particles are large, the absorption efficiencies and asymmetry factors gradually converge to their asymptotic values. The tunneling effect discussed by Baran *et al.* [44], [45] may partially explain the difference of absorption efficiency for the various habits. Mitchell [46] and Mitchell *et al.* [47] discussed and measured the contribution of photon tunneling to extinction and absorption efficiencies.

Bulk ice cloud single-scattering properties are derived by averaging the single-scattering properties of individual ice crystals over 30 particle size distributions adopted from [38]. The average is carried out with respect to the ice crystal maximum dimension, and particles sizes can range from 1–10 000 μm. The wavenumber-dependent bulk extinction efficiencies, absorption efficiencies, and asymmetry factors are parameterized subsequently as functions of the effective particle sizes using the same method as [48].

Fig. 2 shows the mean extinction efficiencies, absorption efficiencies, asymmetry factors, and single-scattering albedos derived from the parameterizations at four wavenumbers: 900, 1102, 1231, and 1587 cm^{-1}. The wavenumber 1102 cm^{-1} is chosen because it is located in the middle of the atmospheric window between 1070–1135 cm^{-1}.

The single-scattering properties of these wavenumbers showed in Fig. 2 are used in following sections to retrieve ice cloud properties. The single-scattering properties for each distribution are strongly dependent on the effective particle size in the IR region, particularly for small sizes and are also sensitive to the wavenumber. The sensitivity to crystal size between those wavenumbers is due fundamentally to the change in complex refractive index for ice between those wavenumbers. Because the wavenumber at 900 cm^{-1} is located in a strong ice absorption band, the absorption efficiency is larger, and the single-scattering albedo is smaller than at other wavenumbers, particularly for particles of small effective diameter. The difference between the single-scattering albedos at 1231 and 900 cm^{-1} increases with decreasing effective particle size. As a result, some information regarding particle size is contained in the BTD between these two channels. The BTD between these two channels has been used to infer particle size by some investigators [49]. The single-scattering properties at 1102, 1231, and 1587 cm^{-1} have similar variations with effective particle size; thus, the ice cloud BTD between these three wavebumbers depends less on effective particle size.

B. Coupling the Fast Cloud Model With the Clear-Sky AIRS Model

The ice cloud reflection and transmission functions can be coupled with the AIRS clear-sky fast radiative transfer model developed by Strow *et al.* [30]. We refer to this combination as the "fast cloud ratiative transfer (RT)" model, which is shown schematically in Fig. 3. In the model, we assume that the clouds are located in a plane-parallel, single homogeneous, and isothermal layer in a given FOV. The vertical arrows in Fig. 3 indicate the isotropic radiation, while the slanted arrows represent radiation that is dependent on the observing zenith angle. The terms $\mathrm{T}_c(\mu)$ and $\mathrm{R}_c(\mu)$ in the figure are transmission and reflection functions of clouds, respectively. $\mu = \cos(\theta_v)$, in which θ_v is the satellite observing zenith angle. The upwelling radiances at the top of the atmosphere (TOA) are composed of the following four parts.

1) The transmission of emission from the lower atmosphere and the surface, and the radiation reflected by the surface $I_0 T_c(\mu) T_{a1}$, in which $\mathrm{T}_c(\mu)$ is the transmission of clouds (including direct transmission and diffuse transmission). I_0 is the upward radiation at cloud-base (including the radiation from the surface, the lower atmosphere, and surface reflectance)

$$I_0 = \varepsilon B(t_s) T_{a01} + \int_{T_{a0}}^{T_{a1}} \frac{B(t)}{T_{a1}} dT_a + (1-\varepsilon) I_0^{\downarrow} T_{a01} \quad (1)$$

where ε is the surface emisivity, and T_a is clear-sky atmospheric transmittance from the TOA to some altitude. T_{a0} is the atmospheric transmittance from the TOA to the surface. T_{a1} is atmospheric transmittance from TOA to cloud-top. T_{a01} is atmospheric transmittance between cloud base and the surface. t_s is the surface temperature. $B(t)$ is the Planck radiance at temperature t, $I_0^{\downarrow}$ is the downward radiation at the surface from the atmosphere and clouds, and $(1-\varepsilon) I_0^{\downarrow}$ is the radiation reflected by the surface. Because the surface reflectance in the IR region is small, only the first-order scattering between the surface and clouds is considered. The multiple-scattering events between the surface and clouds are ignored. The upward radiation below the cloud is assumed to be isotropic in IR region.

2) The radiation emitted from the clouds, denoted as $T_{a1} I_{\mathrm{cld}}$, in which I_{cld} is the cloud radiation given by

$$I_{\mathrm{cld}}(\mu) = \left[1 - R_c(\mu) - T_c(\mu)\right] B(t_c) \quad (2)$$

where $R_c(\mu)$ is the reflectance of the clouds, and t_c is the cloud temperature.

3) The atmospheric radiation emitted above the cloud I_1, given by

$$I_1 = \int_{T_{a1}}^{1} B(t) dT_a. \quad (3)$$

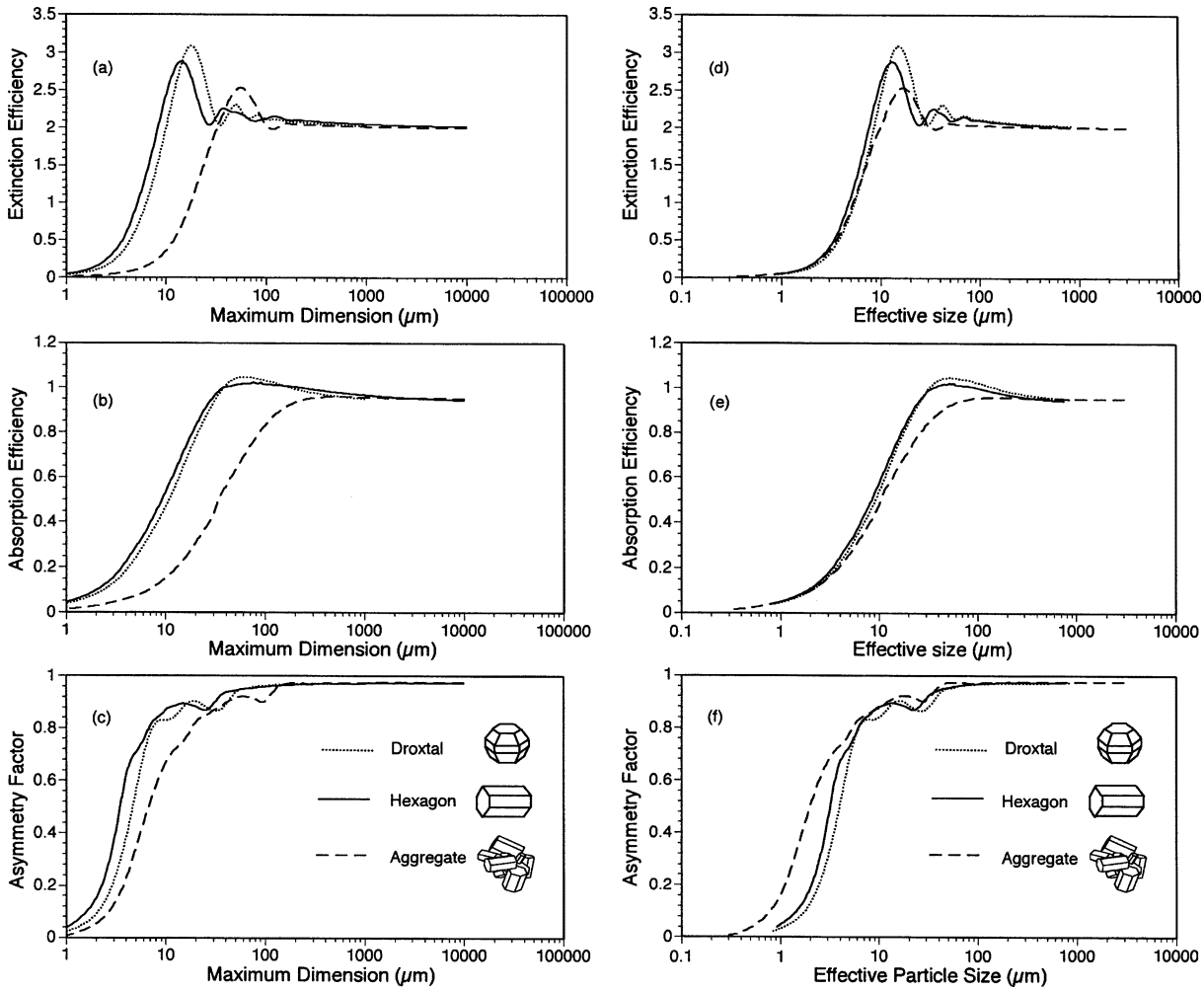

Fig. 1. Comparisons of the single-scattering properties of randomly oriented droxtals, hexagons, and aggregates at a wavenumber of 1250 cm^{-1} as functions of (left) maximum dimension and (right) effective particle size.

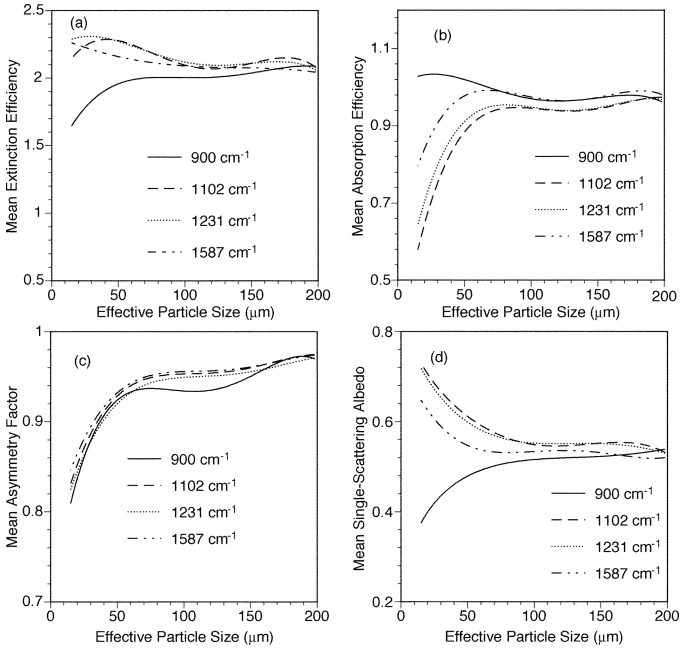

Fig. 2. Parameterized mean extinction efficiency, absorption efficiency, asymmetry factor, and single-scattering albedo as a function of effective diameter for four wavenumbers.

4) The reflected radiation by the clouds from the upper atmosphere $R_c(\mu)T_{a1}I_1^{\downarrow}$, in which the $I_1^{\downarrow}$ is the downward radiation at the top of the cloud

$$I_1^{\downarrow} = I_s \cos(\theta_s) + \int_{T_{a1}}^{1} \frac{T_{a1}}{T_a^2} B(t) dT_a \tag{4}$$

where I_s is the solar radiation. θ_s is solar zenith angle. In the mid-IR region, the contribution from solar radiation is small compared with the radiation emitted from the surface and the atmosphere.

The total radiation at the top of atmosphere is the sum of the four parts

$$I_{\mathrm{TOA}}(\mu) = I_0 T_c(\mu) T_{a1} + I_{\mathrm{cld}}(\mu) T_{a1} + I_1 + I_1^{\downarrow} R_c(\mu) T_{a1}. \tag{5}$$

The downwelling radiation at the surface in (1) is

$$I_0^{\downarrow} = T_{a01}\left[I_1^{\downarrow} T_c(\mu) + I_{\mathrm{cld}}(\mu)\right] + \int_{T_{a0}}^{T_{a1}} B(t) \frac{T_{a0}}{T_a^2} dT_a. \tag{6}$$

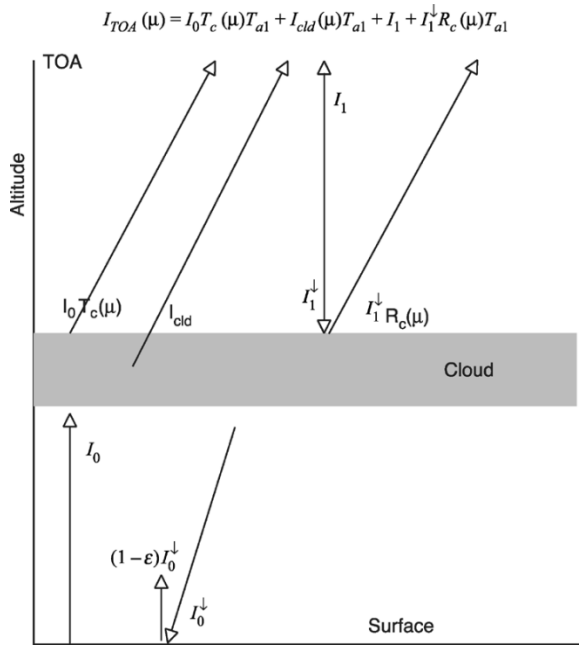

Fig. 3. Schematic of IR radiative transfer in a cloudy atmosphere.

The atmospheric transmittance from the TOA to each layer (T_{ai}) can be calculated from the AIRS clear-sky fast model [30]. Given the observing zenith angle, wavenumber, cloud effective particle size, and optical thickness, the cloud transmission and reflection functions are computed through interpolation using the precomputed database described in Section II-C. The radiance at the top of the atmosphere in direction μ can be efficiently calculated from (1)–(6).

C. Database of Reflection and Transmission Functions for Ice Clouds

If the radiation emitted from the surface and atmosphere below the cloud is isotropic, the ice cloud reflection and transmission functions can be calculated by the DISORT method [28]. Because the ice particle's size parameter is large at a visible wavelength (e.g., 0.55 μm), the extinction efficiency at a visible wavelength is close to the geometric optics asymptotic value of 2. At other wavelengths, the optical thickness can be approximated by

$$\tau(\lambda) = \frac{\langle Q_e(\lambda) \rangle}{2} \tau_{\text{vis}} \tag{7}$$

where $\langle Q_e(\lambda) \rangle$ is the mean extinction efficiency at the wavelength of λ, and τ_{vis} is the ice cloud optical thickness at a visible wavelength (say 0.55 μm). The optical thickness involved in the remainder of the study is defined as being relative to that at the visible wavelength.

Detailed information on the phase function is unnecessary for radiative transfer calculations at IR wavenumbers because the mutiple-scattering effect is only on the order of a few percent. The Henyey–Greenstein (H–G) phase function is often used as an approximation to the phase function in the AIRS IR wavelength region [50], [51]. The H–G phase function can be derived from the parameterization of the asymmetry factor in a straightforward manner. Thus, the single-scattering albedo, optical thickness, and scattering phase function can be derived from the aforementioned parameterizations, given the wavenumber, visible optical thickness, and effective particle size. These single-scattering parameters are input into DISORT for the computation of the reflection and transmission functions. In this manner, a database of reflection and transmission functions is derived at satellite observing zenith angles ranging from 0° to 80°, wavelengths ranging from 3–20 μm, optical thicknesses ranging from 0.04–100, and effective particle sizes ranging from 15–200 μm. The database is prepared in advance and used for fast interpolation during the radiance simulation.

D. Comparisons Between the Fast Cloud Model With DISORT

The fast cloud RT model is validated by comparing the brightness temperatures from this method to the more precise calculations obtained from DISORT. An example involving cloud optical thickness is shown in Fig. 4. The atmospheric profile in the calculation is from the European Center for Medium-Range Weather Forecasts (ECMWF) model data. The cloud-top temperature is assumed to be 222 K, and the surface temperature is 291.4 K. The BTD between DISORT and the fast cloud model is less than 0.5 K (root mean square) for most cloudy cases. Because the database of reflection and transmission functions is precalculated, and the interpolation from the lookup table requires little computational time, the fast model is quite efficient computationally. On the basis of some computations on a desktop workstation (Dell 530), our fast model requires ~0.1 s of CPU time to calculate radiances for a 100-layer atmosphere with one cloud layer for 2378 AIRS channels. It takes 279 s to run 16 streams DISORT for the same set of conditions. The fast model runs more than three orders of magnitude faster than the corresponding DISORT.

III. Sensitivity Studies

In the following discussions, we study the sensitivity of AIRS spectral BTs or BTD to the ice cloud microphysical properties.

A. Optical Thickness

Fig. 5 shows simulated AIRS BT spectra for both clear-sky and ice cloud cases; the ice clouds are given four optical thicknesses but with a fixed effective particle size of 50 μm. In the atmospheric window region, the BT decreases with an increase of cloud optical thickness. The BT decreases more than 70 K as the optical thickness increases from 0–10. The BT varies with wavenumber between 750–1000 cm^{-1} for ice clouds of small to moderate optical thickness due to absorption, and absorption depends on both the wavenumber and effective particle size. Within 1070–1135 cm^{-1}, the BT varies with ice cloud optical thickness. The sensitivity of BT to optical thickness within this wavenumber interval may be used for ice cloud optical thickness retrieval.

The AIRS channels cover a broad spectral range, some of which are located in the atmospheric window region, such as 800–1250 cm^{-1}, or located in regions of strong atmospheric absorption, such as the water vapor band at 1600 cm^{-1} or the CO_2 absorption band at 670 cm^{-1}. The radiances from

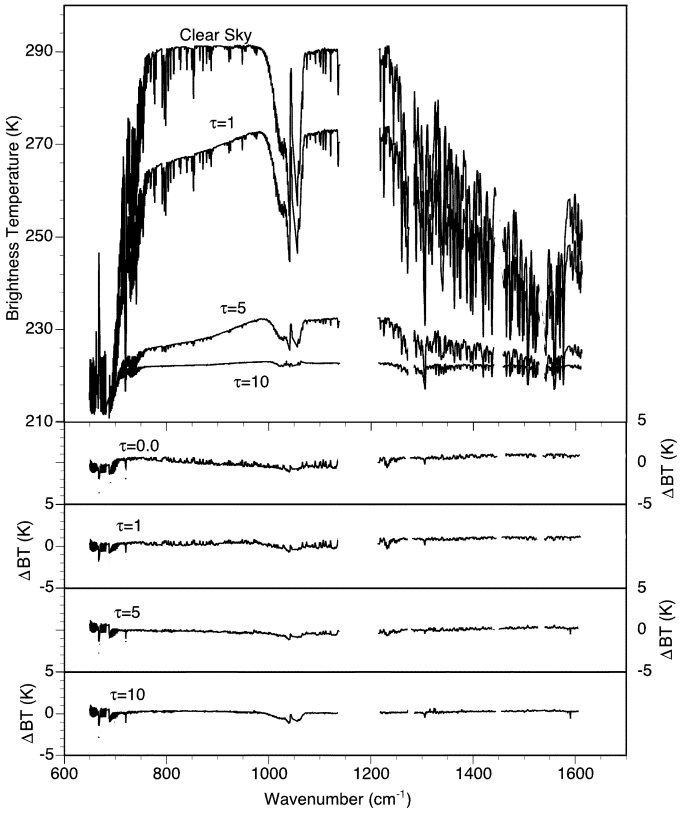

Fig. 4. Brightness temperature spectra calculated using the fast model and deviations relative to the more "exact" DISORT model (ΔBT) for a clear-sky case and three ice cloud optical thicknesses, assuming that the effective particle size is 50 μm, the cloud-top temperature is 222 K, and the surface temperature is 291.4 K.

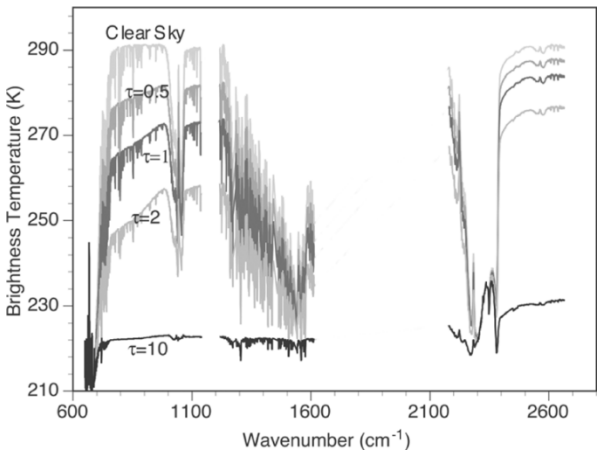

Fig. 5. Simulated upwelling brightness temperature spectra at the top of the atmosphere for a clear-sky case and four ice cloud optical thicknesses (listed in the figure, corresponding to the curves from top to bottom) assuming an effective particle size of 50 μm, a cloud temperature of 222 K, and a surface temperature of 291.4 K.

wavenumbers located in strong absorption bands contain upper atmospheric information. However, radiances at window channels include information from the surface and lower atmosphere, depending on the opacity of any clouds or aerosols that may be present in the column. Four channels marked as A, B, C, and X in Table I are used to study the sensitivity of AIRS

TABLE I
AIRS WAVENUMBER CHANNELS USED IN THE STUDY AND THEIR ABSORPTION FEATURES

	Wavenumber(cm^{-1})	AIRS channel	Ice absorption	Atmospheric Absorption
A	900.562	760	Strong	Weak
B	1231.190	1291	Relatively weak	Weak
C	1587.495	1828	Moderate	Moderately Strong
X	1558.692	1787	Moderate	Strongest

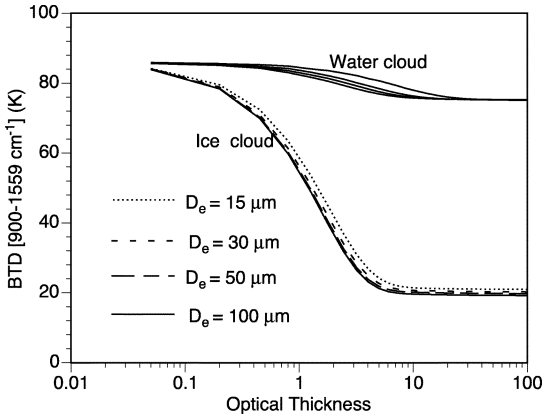

Fig. 6. Variation of the BTD between channel A (900 cm^{-1}) and X (1559 cm^{-1}) with optical thickness, and effective particle size for ice clouds and water clouds (standard tropical atmosphere). Water cloud and ice cloud heights are assumed at 10 and 2 km, respectively.

data to ice cloud properties by using the BTD-based method. The absorption features by the atmosphere and ice crystals of these four channels are also shown in Table I. Channel X is located in a region of strong atmospheric water vapor absorption. The peak of its weighting function is located well above potential clouds, even for the subarctic winter atmospheric model (polar atmosphere). So, this channel provides a reference wavenumber for retrieving cloud optical thickness. Channels A and B are located in the atmospheric window channels; the peaks of their weighting functions are at or very near the surface. Because the absorption by ice is different at these two wavenumbers, the absorption and scattering processes within the clouds have some particle size dependence. This will be discussed further in Section III-B. Channel C is located in a water vapor absorption band, but the absorption is much smaller compared to the channel X. For this reason, we call channel C a "moderate absorption" band. The peak altitude of the weighting function of channel C is above water clouds but below ice clouds (similar to the MODIS 1.38-μm channel). This channel contains negligible information from the lower water clouds. For simplicity, we use 900, 1231, 1587, and 1559 to represent the precise wavenumbers at A, B, C, and X in Table I, respectively, and in the remainder of this paper.

Fig. 6 shows the variation of BTD between channel A and X, denoted as BTD[900-1559] as a function of optical thickness and effective particle size for both water and ice clouds. We use a standard climatological tropical atmosphere and assume heights for water and ice clouds of 2- and 10-km altitude, respectively. The surface temperature is 300 K. Water cloud

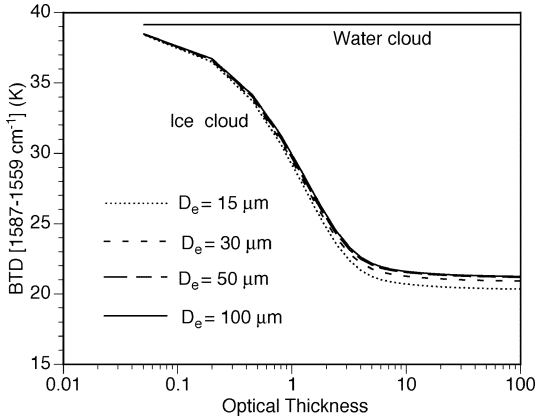

Fig. 7. Same as Fig. 6, but for the BTD between channel C (1587 cm^{-1}) and X (1559 cm^{-1}).

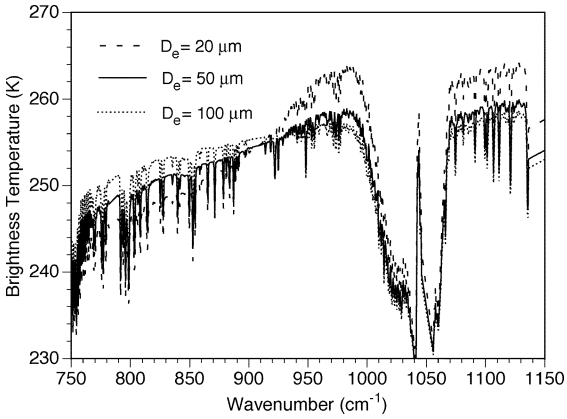

Fig. 8. Simulated upwelling brightness temperature at the top of the atmosphere for three ice cloud effective particle sizes. The optical thickness is fixed at a value of 2.

scattering properties are calculated from Lorenz–Mie theory, assuming Gamma particle size distributions. The BTD[900-1559] is sensitive to optical thickness of ice clouds, with the value of the BTD increasing to more than 60 K as the optical thickness increases from 0–5. The BTD[900-1559] is essentially independent of the effective particle size. Note that the BTD[900-1559] for ice clouds no longer has any sensitivity once the optical thickness becomes larger than 10. As for water clouds, the sensitivity of the BTD optical thickness is much smaller than that for ice clouds, providing an indication that the BTD[900-1559] is not very sensitive to low-level water clouds.

Fig. 7 shows the similar calculations for BTD between channels C and X, denoted as BTD[1587-1559]. Although channel C (1587 cm^{-1}) is located in a water vapor absorption band, the brightness temperature is nearly 40 K higher than for channel X (1559 cm^{-1}) under clear sky conditions. The BTD between channels C and X is also sensitive to optical thickness, but insensitive to effective particle size. The BTD[1587-1559] decreases to 20 K as optical thickness increases from 0–5. Fig. 7 also shows the behavior of the BTD for a water cloud. Since the BTD between these two channels contains no information on lower level water clouds, only the optical thickness of ice clouds is derived from the BTD[1587-1559].

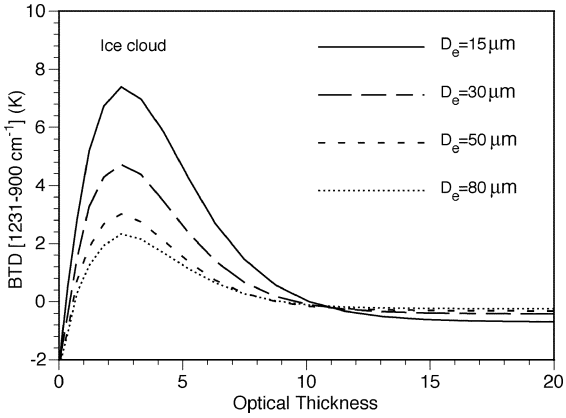

Fig. 9. BTD between channel B and A (BTD1231-900) as a function of ice cloud optical thickness and effective particle size.

The results in Figs. 5–7 may be summarized as follows. Some sensitivity to ice cloud optical thickness is contained in the spectral BTs within the atmospheric windows channels or BTD[900-1559] or BTD[1587-1559]. However, there is little sensitivity to the presence of low-level water clouds.

B. Effective Size

The sensitivity of the BT spectra to the effective particle size is demonstrated in Fig. 8. The slope of the BT at wavenumbers between 790–960 cm^{-1} is sensitive to the effective particle size, especially for small particles. The slope of BT within this wavenumber range increases with a decrease of particle size. But the sensitivity decreases significantly once the effective particle size approaches or exceeds 50 μm. The sensitivity is also related to optical thickness.

One of the widely used retrieval algorithms is the so-called split window technique [16], which is based on the different absorption features of ice at two channels located in the atmospheric window. Ackerman *et al.* [52] studied the BTD between 8–11 μm of aircraft-based IR interferometer observations for retrieving cirrus cloud properties. Similarly, we show the variation of BTD[1231-900] with optical thickness and effective particle sizes of ice clouds in Fig. 9. The BTD between these two channels is relatively insensitive to the optical thickness, but sensitive to small particle sizes for semitransparent ice cloud, since the single-scattering albedoes of ice clouds at these two channels vary differently with effective size for small particle ice clouds [see Fig. 2(d)].

C. Ice Cloud Identification

Because the absorption between channels A and B is greatly different for water and ice clouds, Strabala *et al.* [49] and Baum *et al.* [53] used the BTD between 8.5–11 μm (which is close to the channels B and A defined in present studies) to determine cloud thermodynamic phase. We also calculate the BTD between 1231 and 900 cm^{-1} for water clouds, as shown in Fig. 10. Compared to Fig. 9, Fig. 10 shows that BTD[1231-900] for ice cloud tends to be positive or close to zero when the optical thickness is larger than 0.5, and the BTD[1231-900] for water clouds is always negative and usually less than -2 K. The difference

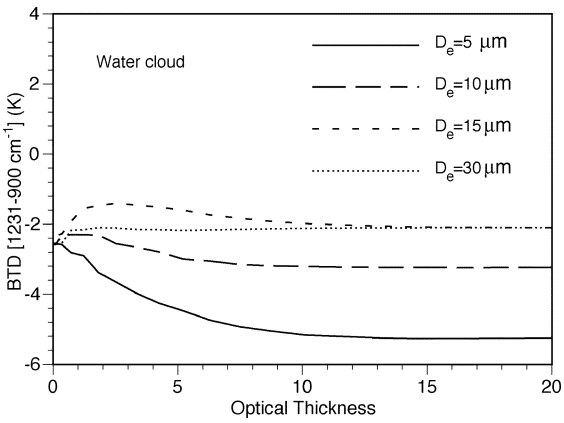

Fig. 10. BTD between channel B and A (BTD1231-900) as a function of water cloud optical thickness and effective particle size.

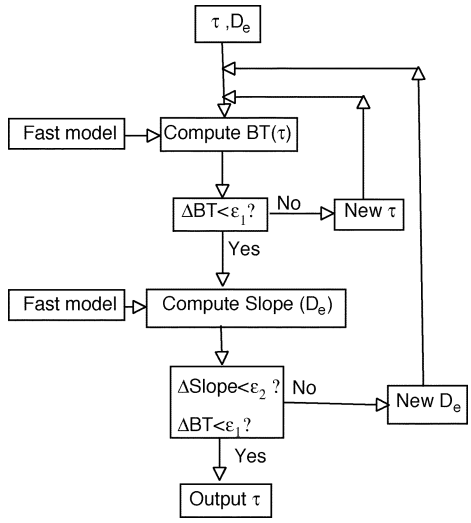

Fig. 11. Flowchart for the retrieval algorithm of ice cloud optical thickness.

of BTD[1231-900] for ice clouds and water clouds is used for identifying the ice cloud FOV in the study (see next section).

IV. Ice Cloud Optical Thickness Retrieval Method and Error Analysis

A. Retrieval Methods

Based on the sensitivity studies in Section III, we develop two approaches to derive ice cloud optical thickness, one based on the spectral BTs within the window and one based on BTDs. In the spectrum-based approach, spectral BTs at atmospheric window channels (1070–1135 cm^{-1}) are used to retrieve ice cloud optical thickness. The slope in brightness temperature between 790–960 cm^{-1} is used to adjust the effective particle size during the retrieval. In the BTD-based method, the BTD[900-1559] and the BTD[1587-1559] are used to retrieve ice cloud optical thickness.

The methodology is applied to an AIRS granule of data, but the retrieval in this paper is limited to the AIRS FOVs where an ice cloud is present. The MODIS bispectral IR approach for thermodynamic phase [7], [53] is used to select FOVs that contain ice clouds for the optical thickness retrieval. Based on the simulation in Figs. 9 and 10, we assume an FOV contains some ice clouds if the BT at 900 cm^{-1} is lower than 238 K, or the BTD[1231-900] is higher than 0.5 K, or the BTD[1231-900] is higher than -0.5 K and BT900 is higher than 285 K.

To simulate the BTs of AIRS observations, atmospheric profiles from the ECMWF gridded meteorological product are collocated to AIRS pixels in time and location. The profiles include the atmospheric temperature, water vapor, and ozone. These atmospheric profiles are interpolated to 101 pressure levels and input to the AIRS fast cloud model to calculate the clear-sky and cloud AIRS radiances. Cloud-top pressure is provided in the MODIS cloud products [7]. The most probable MODIS cloud-top pressure within an AIRS FOV is chosen as a collocated cloud-top pressure.

The flowchart for retrieving ice cloud optical thickness is shown in Fig. 11. Given an initial optical thickness and effective particle size, the mean brightness temperature difference ΔBT between the observed and simulated from 1070–1135 cm^{-1} is computed using the fast cloud model. The ice cloud optical thickness is adjusted until ΔBT is below a threshold ($\varepsilon_1 =$ 0.05 K), resulting in a "first guess" optical thickness. Subsequently, the effective particle size is adjusted until the simulated slope between 790–960 cm^{-1} matches the observed slope. The final ice optical thickness is produced when both the simulated BTs between 1070–1135 cm^{-1} and the slope between 790–960 cm^{-1} match the measurements.

The BTD-based retrieval procedure, using the BTD[900-1559] or BTD[1587-1559], are almost the same as the retrieval procedure from the spectrum-based approach mentioned in the previous paragraph, except that the mean difference between observed and simulated BTs from 1070–1135 cm^{-1} is replaced by the difference between simulated and AIRS observed BTD[900-1559] and BTD[1587-1559], respectively. Finally, the results based on the BTD[900-1559] are used for the comparison with MODIS.

B. Error Analysis

The accuracy of the retrieved cloud optical thickness depends on the accuracy of both measurements and simulations, which involve both the radiative transfer model and cloud single-scattering properties. A number of factors will affect the model accuracy, such as uncertainty in the surface temperature, surface emissivity, cloud-top temperature, and atmospheric profiles, along with the inhomogeneous and partial cloudiness within a pixel. Partial and inhomogeneous cloudiness within a FOV is not considered in the present fast cloud radiative transfer model. Thus, the result from application of our model is the average optical thickness over an AIRS FOV. The uncertainty of the clear-sky fast model is less than 0.1 K within atmospheric window channels [30]. The uncertainty of our fast cloud model is generally within 0.5 K. Thus, the most uncertainty in the inferred optical thickness probably stems from the errors of atmospheric profile, cloud-top temperature, and the surface temperature.

Huang *et al.* [21] studied the effects of surface temperature and cloud temperature on the retrieved accuracy of cloud optical thickness using airborne IR spectral observations. The general conclusions of their study are as follows. The error of cloud-top

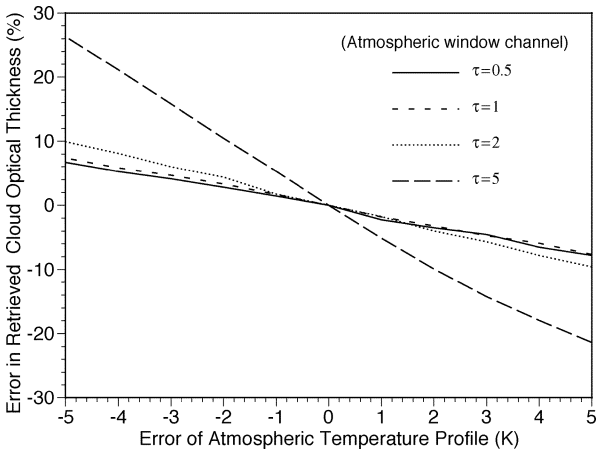

Fig. 12. Errors in retrieved optical thickness inferred using the IR atmospheric channel BTs resulting from an error in atmospheric profile for four ice cloud optical thicknesses.

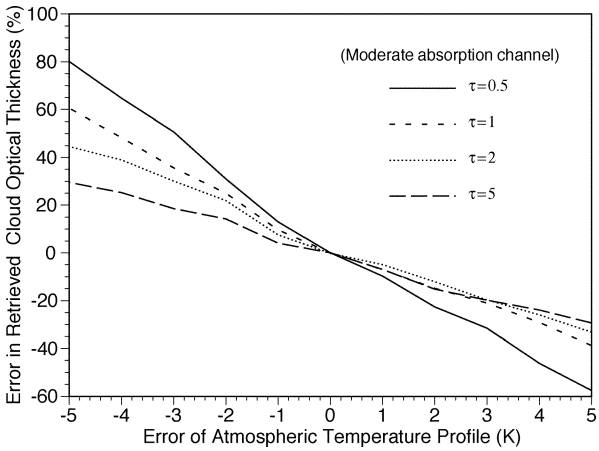

Fig. 13. Same as Fig. 12, except that the results are derived using the moderate absorption channel.

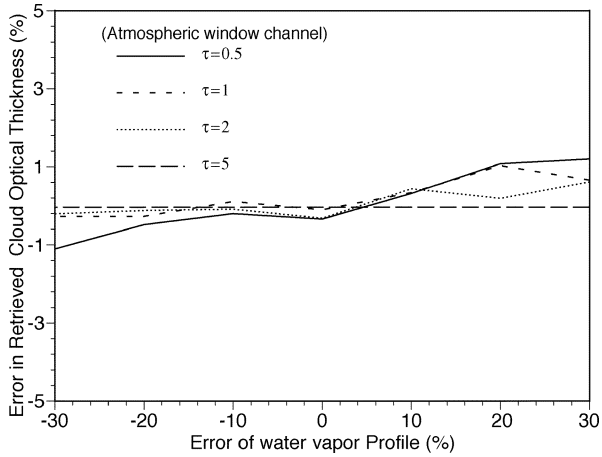

Fig. 14. Sensitivity of the error in retrieved optical thickness determined using the atmospheric window channel to a simulated error in the atmospheric water vapor profile.

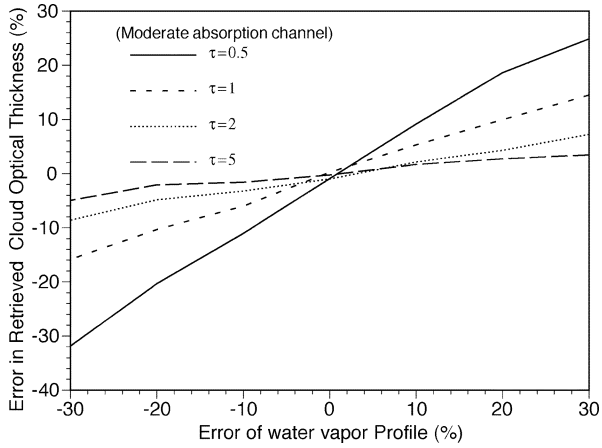

Fig. 15. Same as Fig. 14, except that the results are derived using the moderate absorption channel.

temperature has less influence on the retrieval of optical thickness for optically thin clouds than for optically thick ice clouds. The error in the retrieved optical thickness is less than 10% if the cloud temperature is within ± 5 K of the true temperature, and the cloud optical thickness is less than 2. Error in the surface temperature has little influence when optically thick clouds are present, but becomes important for optically thin clouds. To have a retrieval accuracy to be better than 10% for optical thickness, the surface skin temperature error needs to be less than ± 2.5 K when cloud optical thickness is larger than 1.

There will be additional errors in the retrieved optical thickness associated with uncertainties in atmospheric temperature and water vapor profiles. To investigate an extreme scenario, we assume an uncertainty in the atmospheric temperature profile of ± 5 K for each layer, and an error of $\pm 30\%$ in water vapor for each layer. Subsequently, the resulting cloud optical thicknesses are compared with the counterpart assuming that the temperature and humidity profiles are known exactly.

Fig. 12 shows the error in the retrieved optical thickness derived using the BTD[900-1559] as a function of the error of atmospheric temperature profile. An error in the atmospheric temperature profile has a more pronounced influence on the retrieval of optical thickness for an optically thick cloud than for an optically thin cloud. However, if the uncertainty in the atmospheric temperature profile is within ± 2 K and the ice cloud optical thickness is less than 5, the uncertainty in the retrieved optical thickness is within $\pm 10\%$.

With the optical thickness derived using the moderate absorption channel BTD[1587-1559], as shown in Fig. 13, the retrieved error increases with a decrease of cloud optical thickness. The moderate absorption channel approach is more sensitive than the atmospheric window channel approach to the uncertainties in the atmospheric temperature profile. For optically thin cloud, the error in the retrieved optical thickness can be more than $\pm 50\%$.

Error in the atmospheric water vapor profile has little influence on the error of the retrieved optical thickness using the atmospheric window channel BTD[900-1559], as shown in Fig. 14, but has a considerable influence on the moderate absorption channel results from analysis of the BTD[1587-1559], particularly for optically thin cloud as shown in Fig. 15. In summary, uncertainties in the atmospheric profiles have a minor effect on the IR atmospheric window channel retrievals, but have a pronounced influence on the moderate absorption channel retrievals.

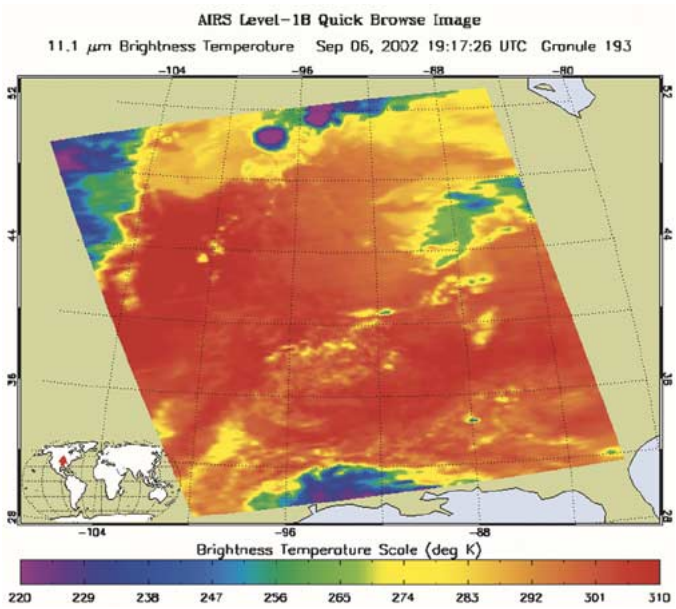

Fig. 16. Image derived using the AIRS brightness temperature for channel 760 (11.1 μm, 900.562 cm^{-1}).

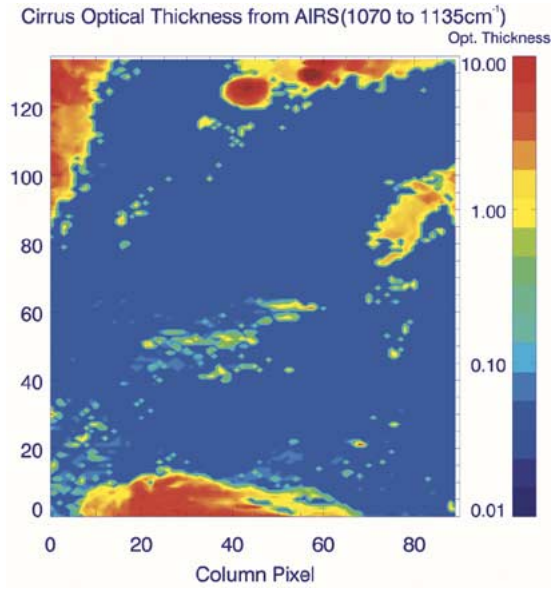

Fig. 17. Ice cloud optical thickness retrieved using AIRS 1070–1135 cm^{-1} spectral data.

V. Case Study

The preceding methodology is applied to an entire granule of AIRS data. Fig. 16 is an image of the channel 760 (11.1 μm; 900.562 cm^{-1}) brightness temperatures at 1917 UTC on September 6, 2002. The center of the image is located at (94°W, 42°N) over the central United States. There are 90 × 135 FOVs in the granule. The solar zenith angle ranges from 24.6° to 51.6°. The satellite scanning zenith angle ranges from 0° to 57.1°. Our analyses are limited to the AIRS FOVs where ice clouds are present. The FOVs of ice clouds are determined by analysis of the BT at 900 cm^{-1} and BTD[1231-900] as discussed earlier. We assume a land-model surface spectral emission in the retrieval. The emissivity varies between 0.91 and 0.998 in IR 500–3000 cm^{-1}. The retrievals of optical thickness are based on the AIRS BTs or BTDs for the following spectral region and bands: 1) 1070–1135 cm^{-1} spectral data; 2) 900 and 1559 cm^{-1}; and 3) 1587 and 1559 cm^{-1}, respectively. The retrieved optical thickness based on BTD[900-1559] is compared with the results from MODIS 0.645- and 1.38-μm bands.

A. Spectrum-Based Ice Cloud Optical Thickness Retrieval

Fig. 17 shows the retrieved ice clouds optical thickness derived from data within the 1070–1135 cm^{-1} spectral region. The horizontal and vertical axes in Fig. 17 indicate crosstrack and along-track FOVs in the AIRS granule, respectively. The optical thickness results in Fig. 17 and subsequent figures are provided using a logarithmic scale to better display the range of values. In some FOVs, the optical thickness is much larger (red or dark red pixels), indicating areas of convection.

Fig. 18 shows comparisons between simulated and observed AIRS spectral BTs for two FOVs. The brightness temperature differences between observations and simulations are also shown in the bottom panels of Fig. 18. One FOV [upper curves in Fig. 18(a) and (b)] contains extremely thin cirrus, and the

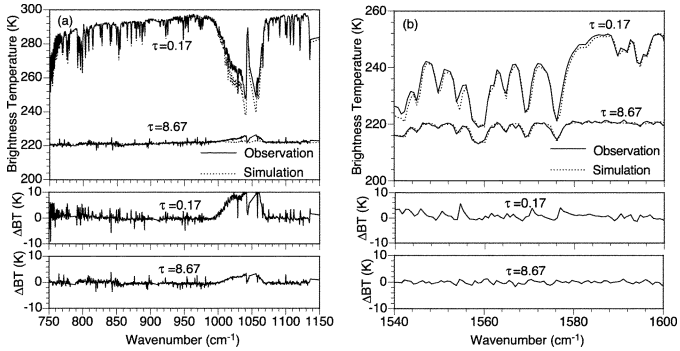

Fig. 18. Comparisons between simulated and observed AIRS spectral BTs for clear and cloudy sky scenes within (a) an atmospheric window band and (b) the water vapor (strong absorption) band. The brightness temperature differences (ΔBT) between observations and simulations are also shown.

retrieved optical thickness is 0.17. The other FOV [lower curves in Fig. 18(a) and (b)] is chosen from an optically thick ice cloud where the retrieved optical thickness is 8.67. The BTs for the atmospheric window channels are at about 220 K, and there are no atmospheric molecular absorption features. Fig. 18(a) shows the comparison of simulated to observed cloud radiances within the atmospheric window channels (750–1135 cm^{-1}). The simulated BT compares well with observed AIRS data both for clear and cloudy skies except in the 9.6 μm O_3 absorption band and is probably due to limitations in the ECMWF model fields. Within a strong water vapor absorption band (e.g., 6.2 μm) shown in Fig. 18(b), the agreement between the simulated BTs and observed BTs is still close, although the variation in BT due to ice clouds is much smaller than in the window channels.

The retrieval based on the BTD[900-1559] provides similar optical thickness results to those in Fig. 17. Fig. 19 shows a scatterplot based on a comparison of retrieved optical thickness from AIRS atmospheric window spectral channels (1070–1135 cm^{-1}) to values based on AIRS BTD[900-1559]. Basically, the retrieved results from our spectrum-based approach and

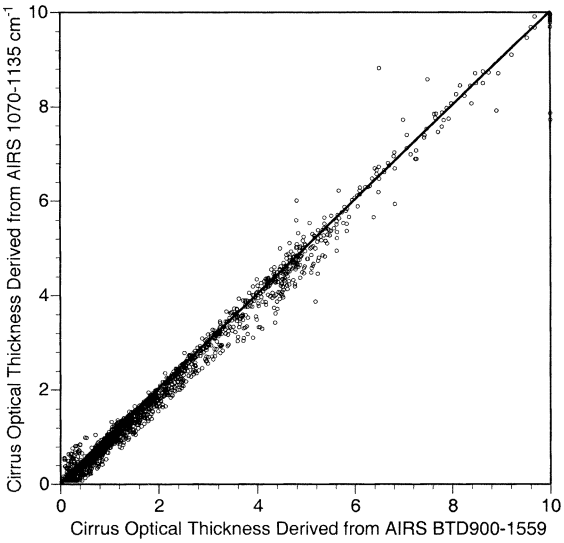

Fig. 19. Comparison of the ice cloud optical thickness retrieved from AIRS atmospheric window spectral channels (1070–1135 cm^{-1}) and the AIRS BTD[900-1559].

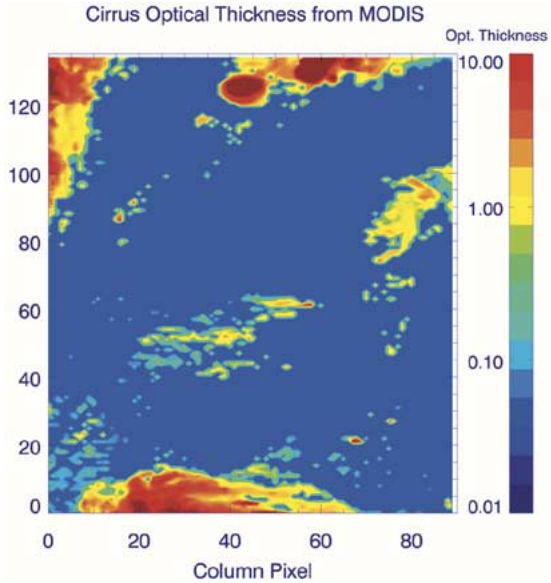

Fig. 20. Retrieved ice cloud optical thickness inferred from use of the MODIS 0.645- and 1.38-μm bands.

the BTD-based method compare well with each other; the deviation (root mean square) is 0.115.

B. Comparison of AIRS With MODIS Optical Thickness Retrievals

It is useful to compare the AIRS-derived optical thickness with that derived from the MODIS 0.645- and 1.38- μm reflectance bands [14]. In this study, we have chosen to use these two bands rather than the operational product based on the 0.645-, 1.6-, and 2.1-μm bands discussed by Platnick *et al.* [7]. The 1.38-μm band is quite sensitive to upper level clouds. Meyer *et al.* [15] developed a method to retrieve the optical thickness of tropical ice clouds using MODIS 0.645- and 1.38-μm reflectances. In their approach, an optical thickness lookup library is generated using previously calculated single-scattering data in conjunction with the DISORT radiative transfer model. The inference of optical thickness for each pixel in a MODIS granule is based on this lookup library. The MODIS nadir spatial resolution for the 0.645- and 1.38-μm bands is 1 km, whereas the AIRS spatial resolution is 13.5 km. To compare the MODIS and AIRS results, MODIS optical thicknesses are collocated with each AIRS FOV and degraded to match the AIRS spatial resolution [54] by averaging the optical thickness over all MODIS pixels within each AIRS FOV. An AIRS FOV can include up to 250 MODIS pixels. Fig. 20 shows the spatially degraded mean ice cloud optical thickness image derived from MODIS 1.38- and 0.645-μm channels. From comparison of Fig. 17 and Fig. 20, it may be seen that the overall features of the AIRS retrieved ice cloud optical thicknesses and MODIS results are in reasonable agreement. Fig. 21 shows a scatterplot comparing the ice cloud optical thickness from MODIS and AIRS BTD[900-1559]. The retrieved optical thickness from AIRS coincides with that from MODIS for thin to moderate thick cirrus clouds (optical thickness less than 5). Retrieved optical thickness for AIRS tends to be smaller compared to MODIS as optical thickness increases. This is may be due to the saturation of the BTD signal for large optical

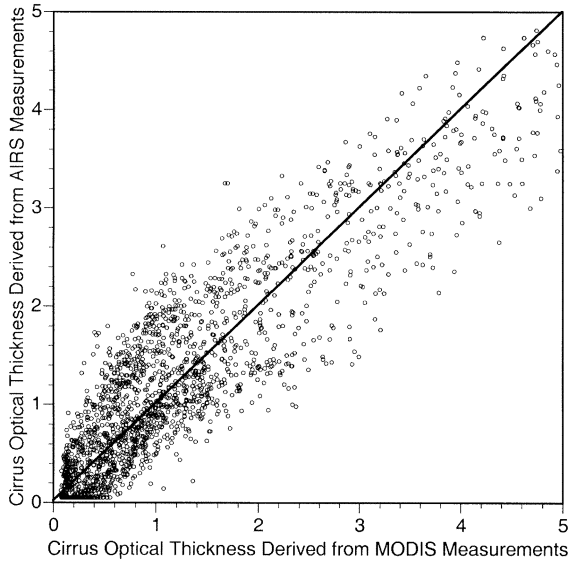

Fig. 21. Comparison of the ice cloud optical thickness values between the MODIS retrievals and the AIRS BTD[900-1559] retrievals.

thickness values (see Fig. 6). For optically thin ice clouds, the points show greater scatter, indicating greater uncertainty in the results. The scattering may be due to the random error of cloud temperature, surface temperature, inhomogeneous and subscale clouds, the error of collocated pixels, and measurement noise, etc.

The optical thickness retrieved from the BTD[1587-1559] (not shown here) has similar results with those from the atmospheric window channels for ice clouds of moderate optical thickness, i.e., when the optical thickness is larger than 1. But differences do exist for those FOVs that contain optically thin clouds. Upon further investigation, we found disagreements between the simulated and observed AIRS BTs. One possibility that may be causing this disagreement is that the atmospheric profiles provided by the ECMWF product at altitudes of about

5–10 km (the altitude of weighting function of this moderate absorption channel) may not represent the true atmospheric condition. As shown in Section IV, the retrieved optical thickness from the moderate absorption channel is more sensitive to uncertainties in the atmospheric profile and water vapor profile (see Figs. 13 and 15).

VI. Discussion and Summary

In this study, we demonstrate the use of AIRS data for inferring ice cloud optical thickness. The retrievals involving atmospheric window channels have a stronger sensitivity to ice cloud optical thickness and are relatively insensitive to the cloud particle size and the error in atmospheric profiles. The results from a moderate absorption channel is primarily sensitive to the presence of ice clouds, but is more sensitive to uncertainties in the atmospheric temperature and water vapor profiles.

There are some restrictions to the application of the present methods. The ice cloud signal in the AIRS data tends to saturate when the optical thickness is larger than 5. This implies that the retrieval of optical thickness from AIRS IR data is only suitable for nonopaque ice clouds. Additionally, IR BT calculations are sensitive to the profiles of the atmospheric temperature and water vapor profiles, particularly for simulations in a strong absorption band. Within atmospheric window channels, the surface temperature is also important for optically thin clouds. Because of the spatial and time mismatch of ECMWF and AIRS data, the profiles of ECMWF data may not be accurate enough to be used for retrieving optical thickness based on the BTD between moderate absorption and strong absorption bands. Perhaps the AIRS-derived profiles of atmospheric temperature and moisture could be used to improve the accuracy using the moderate absorption channel.

A fast cloud radiative transfer model was developed to simulate AIRS radiances when clouds are present. The fast cloud radiance model includes consideration of the single-scattering properties of mixtures of ice crystals and their subsequent parameterizations, a database of transmission and reflection functions for ice clouds calculated from DISORT, and a radiative transfer algorithm coupled with the existing AIRS clear-sky fast model. Compared with DISORT, the discrepancy of the fast cloud model is within 0.5 K (root mean square) in BT. However, the computation is three orders of magnitude faster than DISORT in terms of CPU time requirements and allows the inference of ice cloud properties in AIRS data in a timely manner.

We investigate the sensitivity of AIRS spectral BTs and BTD values between pairs of wavenumbers to the cloud optical thickness. The spectral BTs in the atmospheric window channels within 1070–1135 cm^{-1}, and the BTD between 900.562 cm^{-1} (located in an atmospheric window) and 1558.692 cm^{-1} (located in a strong water vapor absorption band) are sensitive to the ice cloud optical thickness. Similarly, the BTD between a moderate absorption channel (1587.495 cm^{-1}) and a strong water absorption channel (1558.692 cm^{-1}) is sensitive to ice cloud optical thickness, but insensitive to the presence of low-level water clouds. Neither of the aforementioned BTD pairs is sensitive to the effective particle size. The optical thickness of thin to moderately thick ice cloud (optical thickness less than 5) can be retrieved using the method.

A case study regarding the retrieval of optical thickness from a granule of AIRS data is reported. The ECMWF atmospheric profiles are used in the retrieval process to generate atmospheric absorption properties. The retrieved ice clouds optical thickness for each AIRS FOV that contains ice clouds is compared with the collocated and degraded MODIS optical thickness retrieved from the MODIS 1.38- and 0.645-μm channels. The retrieved ice cloud optical thicknesses from the AIRS IR atmospheric window channels compare well with MODIS for the thin to moderately thick ice clouds.

Acknowledgment

The authors thank F. Sun for providing collocated MODIS and AIRS data and appreciate the helpful suggestions from the two anonymous reviewers.

References

[1] D. P. Wylie, W. P. Menzel, H. M. Woolf, and K. L. Strabala, "Four years of global cirrus cloud statistics using HIRS," *J. Clim.*, vol. 7, pp. 1972–1986, 1994.

[2] K. N. Liou, "Influence of cirrus clouds on weather and climate processes: A global perspective," *Mon. Weather Rev.*, vol. 114, pp. 1167–1199, 1986.

[3] G. L. Stephens, S.-C. Tsay, P. W. Stackhouse, and P. J. Flatau, "The relevance of the microphysical and radiative properties of cirrus clouds to climate and climatic feedback," *J. Atmos. Sci.*, vol. 47, pp. 1742–1753, 1990.

[4] D. K. Lynch, K. Sassen, D. O. Starr, and G. Stephens, Eds., *Cirrus*. New York: Oxford Univ. Press, 2002.

[5] T. Nakajima and M. D. King, "Determination of the optical thickness and effective particle radius of clouds from reflected solar radiation measurements. Part I: Theory," *J. Atmos. Sci.*, vol. 47, pp. 1878–1893, 1990.

[6] M. D. King, W. P. Menzel, Y. J. Kaufman, D. Tanré, B. C. Gao, S. Platnick, S. A. Ackerman, L. A. Remer, R. Pincus, and P. A. Hubanks, "Cloud and aerosol properties, precipitable water, and profiles of temperature and humidity from MODIS," *IEEE Trans. Geosci. Remote Sensing*, vol. 41, pp. 442–458, Feb. 2003.

[7] S. Platnick, M. D. King, S. A. Ackerman, W. P. Menzel, B. A. Baum, J. C. Riédi, and R. A. Frey, "The MODIS cloud products: Algorithms and examples from Terra," *IEEE Trans. Geosci. Remote Sensing*, vol. 41, pp. 459–473, Feb. 2003.

[8] S. C. Ou, K. N. Liou, M. D. King, and S. C. Tsay, "Remote sensing of cirrus cloud parameters based on a 0.63–3.7 μm radiance correlation technique applied to AVHRR data," *Geophys. Res. Lett.*, vol. 26, pp. 2437–2440, 1999.

[9] S. C. Ou, K. N. Liou, Y. Takano, G. J. Higgins, A. George, and R. Slonaker, "Remote sensing of cirrus cloud optical thickness and effective particle size for the National Polar-orbiting Operational Environmental Satellite System Visible/Infrared Imager Radiometer Suite: Sensitivity to instrument noise and uncertainties in environmental parameters," *Appl. Opt.*, vol. 42, pp. 7202–7214, 2004.

[10] P. Minnis, K. N. Liou, and Y. Takano, "Inference of cirrus cloud properties using satellite-observed visible and infrared radiances, Part I: Parameterization of radiance fields," *J. Atmos. Sci.*, vol. 50, pp. 1279–1304, 1993.

[11] P. Minnis, P. W. Heck, and D. F. Young, "Inference of cirrus cloud properties using satellite-observed visible and infrared radiances. Part II: Verification of theoretical cirrus radiative properties," *J. Atmos. Sci.*, vol. 50, pp. 1305–1322, 1993.

[12] A. J. Baran, S. Havemann, P. N. Francis, and P. D. Watts, "A consistent set of single-scattering properties for cirrus cloud: Tests using radiance measurements from a dual-viewing multi-wavelength satellite-based instrument," *J. Quant. Spectrosc. Radiat. Transf.*, vol. 79, pp. 549–567, 2003.

[13] M. Doutriaux-Boucher, J. C. Buriez, G. Brogniez, L. Labonnote, and A. J. Baran, "Sensitivity of retrieved POLDER directional cloud optical thickness to various ice particle models," *Geophys. Res. Lett.*, vol. 27, pp. 109–112, 2000.

[14] B. C. Gao, P. Yang, W. Han, R.-R. Li, and W. J. Wiscombe, "An algorithm using visible and 1.38-μm channels to retrieve cirrus cloud reflectances from aircraft and satellite data," *IEEE Trans. Geosci. Remote Sensing*, vol. 40, pp. 1659–1688, Aug. 2002.

[15] K. Meyer, P. Yang, and B.-C. Gao, "Optical thickness of tropical cirrus clouds derived from the MODIS 0.645- and 1.38-μm channels," *IEEE Trans. Geosci. Remote Sensing*, vol. 42, pp. 833–841, Apr. 2004.

[16] T. Inoue, "On the temperature and effective emissivity determination of semi-transparent cirrus clouds by bispectral measurements in the 10 micron windows region," *Meteorol. Soc. Jpn.*, vol. 63, pp. 88–99, 1985.

[17] C. Prabhakara, R. S. Fraser, G. Dalu, M.-L. Wu, and R. J. Curran, "Thin cirrus clouds-seasonal distribution over oceans deduced from Nimus-4 IRIS," *J. Appl. Meteorol.*, vol. 27, pp. 379–399, 1988.

[18] F. Parol, J. C. Buriez, G. Brognies, and Y. Fouquart, "Information content of AVHRR channels 4 and 5 with respect to particle size," *J. Appl. Meteorol.*, vol. 30, pp. 973–984, 1991.

[19] H. H. Aumann, M. T. Chahine, C. Gautier, M. D. Goldberg, E. Kalnay, L. M. McMillin, L. M. H. Revercomb, P. W. Rosenkranz, W. L. Smith, D. H. Staelin, L. L. Strow, and J. Susskind, "AIRS/AMSU/HSB on the Aqua mission: Design, science objectives, data products, and processing systems," *IEEE Trans. Geosci. Remote Sensing*, vol. 41, pp. 253–264, Feb. 2003.

[20] J. Susskind, C. D. Barnet, and J. M. Blaisdell, "Retrieval of atmospheric and surface parameters from AIRS/AMSU/HSB data in the presence of clouds," *IEEE Trans. Geosci. Remote Sensing*, vol. 41, pp. 390–409, Feb. 2003.

[21] A. H. Huang, P. Yang, H.-L. Wei, B. A. Baum, Y.-X. Hu, P. Antonelli, and S. A. Ackerman, "Retrieval of ice cloud properties from high spectral resolution infrared observations," *IEEE Trans. Geosci. Remote Sensing*, vol. 42, pp. 842–853, Apr. 2004.

[22] S. Chung, S. Ackerman, P. F. Van Delst, and W. P. Menzel, "Model calculations and interferometer measurements of ice-clouds characteristics," *J. Appl. Meteorol.*, vol. 39, pp. 634–644, 2000.

[23] J. Bantges, J. E. Russell, and J. D. Haigh, "Cirrus cloud top-of-atmosphere radiance spectra in the thermal infrared," *J. Quant. Spectrosc. Radiat. Transf.*, vol. 63, pp. 487–498, 1999.

[24] S. DeSouza-Machado, L. Strow, S. Hanon, and J. Gou, "Measurements of cirrus cloud parameters using AIRS," *Proc. SPIE*, vol. 5235, pp. 49–58, 2003.

[25] B. H. Kahn, A. Eldering, S. A. Clough, E. J. Fetzer, E. Fishbein, M. R. Gunson, S. Y. Lee, P. F. Lester, and V. J. Realmuto, "Near micron-sized cirrus cloud particles in high-resolution infrared spectra: An orographic case study," *Geophys. Res. Lett.*, vol. 30, pp. 24.1–24.4, 2003.

[26] X. L. Huang, Y. L. Yung, and J. S. Margolis, "Use of high-resolution measurements for the retrieval of temperature and gas concentration profiles from outgoing infrared spectra in the presence of cirrus clouds," *Appl. Opt.*, vol. 42, pp. 2155–2165, 2003.

[27] S. A. Clough, M. J. Tacono, and J. L. Moncet, "Line-by-line calculations of atmospheric fluxes and cooling rates: Application to water vapor," *J. Geophys. Res.*, vol. 97, pp. 15 761–15 785, 1992.

[28] K. Stamnes, S.-C. Tsay, W. Wiscombe, and K. Jayaweera, "Numerically stable algorithm for discrete-ordinate-method radiative transfer in multiple scattering and emitting layered media," *Appl. Opt.*, vol. 27, pp. 2502–2509, 1988.

[29] L. L. Strow, H. E. Motteler, R. G. Benson, S. E. Hannon, and S. Souza-Machado, "Fast computation of monochromatic infrared atmospheric transmittances using compressed look-up tables," *J. Quant. Spectrosc. Radiat. Transf.*, vol. 59, pp. 481–493, 1998.

[30] L. L. Strow, S. E. Hannon, S. Souza-Machado, H. E. Motteler, and D. Tobin, "An overview of the AIRS radiative transfer model," *IEEE Trans. Geosci. Remote Sensing*, vol. 41, pp. 303–313, Feb . 2003.

[31] E. Fishbein, C. B. Farmer, S. L. Granger, D. T. Gregorich, M. R. Gunson, S. E. Hannon, M. D. Hofstadter, S. Y. Lee, S. S. Leroy, and L. L. Strow, "Formulation and validation of simulated data for the Atmospheric Infrared Sounder (AIRS)," *IEEE Trans. Geosci. Remote Sensing*, vol. 41, pp. 314–329, Feb. 2003.

[32] M. I. Mishchenko, W. B. Rossow, A. Macke, and A. A. Lacis, "Sensitivity of cirrus cloud albedo, bidirectional reflectance, and optical thickness retrieval to ice-particle shape," *J. Geophys. Res.*, vol. 101, pp. 16 973–16 985, 1996.

[33] J. Heymsfield and J. Iaquinta, "Cirrus crystal terminal velocities," *J. Atmos. Sci.*, vol. 5, pp. 916–938, 2000.

[34] P. Yang, B. A. Baum, A. J. Heymsfield, Y. X. Hu, H.-L. Huang, S.-C. Tsay, and S. Ackerman, "Single-scattering properties of droxtals," *J. Quant. Spectrosc. Radiat. Transf.*, vol. 79–80, pp. 1159–1169, 2003.

[35] M. I. Mishchenko, J. W. Hovenier, and L. D. Travis, Eds., *Light Scattering by Nonspherical Particles: Theory, Measurements, and Applications*. San Diego, CA: Academic, 2000.

[36] P. Yang and K. N. Liou, "Finite-difference time domain method for light scattering by small ice crystals in three-dimensional space," *J. Opt. Soc. Amer.*, vol. A13, pp. 2072–2085, 1996.

[37] P. Yang, K. N. Liou, M. I. Mishchenko, and B.-C. Gao, "An efficient finite difference time domain scheme for light scattering by dielectric particles: Application to aerosols," *Appl. Opt.*, vol. 39, pp. 3727–3737, 2000.

[38] Q. Fu, P. Yang, and W. B. Sun, "An accurate parameterization of the infrared radiative properties of cirrus clouds for climate models," *J. Clim.*, vol. 25, pp. 2223–2237, 1998.

[39] Q. Fu, W. B. Sun, and P. Yang, "On modeling of scattering and absorption by cirrus nonspherical ice particles at thermal infrared wavelengths," *J. Atmos. Sci.*, vol. 56, pp. 2937–2947, 1999.

[40] P. Yang and K. N. Liou, "Geometric-optics-integral-equation method for light scattering by nonspherical ice crystals," *Appl. Opt.*, vol. 35, pp. 6568–6584, 1996.

[41] P. Yang, B. C. Gao, B. A. Baum, Y. X. Hu, W. J. Wiscombe, S. C. Tsay, D. M. Winker, and S. L. Nasiri, "Radiative properties of cirrus clouds in the infrared (8–13 μm) spectral region," *J. Quant. Spectrosc. Radiat. Transf.*, vol. 70, pp. 473–504, 2001.

[42] Z. Zhang, P. Yang, G. W. Kattawar, S.-C. Tsay, B. A. Baum, H.-L. Huang, Y. X. Hu, A. J. Heymsfield, and J. Reichardt, "Geometric optics solution to light scattering by droxtal ice crystals," *Appl. Opt.*, vol. 43, pp. 2490–2499, 2004.

[43] P. Yang and K. N. Liou, "Single-scattering properties of complex ice crystals in terrestrial atmosphere," *Contr. Atmos. Phys.*, vol. 71, pp. 223–248, 1998.

[44] A. J. Baran, P. N. Francis, and P. Yang, "A process study of the dependence of ice crystal absorption on particle geometry: Application to aircraft radiometric measurements of cirrus cloud in the terrestrial window region," *J. Atmos. Sci.*, vol. 60, pp. 417–427, 2003.

[45] A. J. Baran, S. Haveman, P. N. Francis, and P. Yang, "A study of the absorption and extinction properties of hexagonal ice columns and plates in random and preferred orientation, using exact T-matrix theory and aircraft observations of cirrus," *J. Quant. Spectrosc. Radiat. Transf.*, vol. 70, pp. 505–518, 2001.

[46] D. L. Mitchell, "Effective diameter in radiation transfer: General definition, applications and limitations," *J. Atmos. Sci.*, vol. 59, pp. 2330–2346, 2002.

[47] D. L. Mitchell, W. P. Arnott, C. Schmitt, A. J. Baran, S. Havemann, and Q. Fu, "Contributions of photon tunneling to extinction in laboratory grown hexagonal columns," *J. Quant. Spectrosc. Radiat. Transf.*, vol. 70, pp. 761–776, 2001.

[48] P. Yang, M. G. Mlynczak, H. L. Wei, D. P. Kratz, B. A. Baum, Y. X. Hu, W. J. Wiscombe, A. Heidinger, and M. I. Mishchenko, "Spectral signature of cirrus clouds in the far-infrared region: Single-scattering calculation and radiative sensitivity study," *J. Geophys. Res.*, vol. 108, pp. 4569–4584, 2003.

[49] K. I. Strabala, S. A. Ackerman, and W. P. Menzel, "Cloud properties inferred from 8–12 μm data," *J. Appl. Meteorol*, vol. 33, pp. 212–229, 1994.

[50] D. D. Turner, S. A. Ackerman, B. A. Baum, H. E. Revercomb, and P. Yang, "Cloud phase determination using ground-based AERI observations at SHEBA," *J. Appl. Meteorol.*, vol. 42, pp. 701–715, 2003.

[51] T. J. Garrett, L. F. Radke, and P. V. Hobbs, "Aerosol effects on cloud emissivity and surface longwave heating in the arctic," *J. Atmos. Sci.*, vol. 59, pp. 769–778, 2002.

[52] S. A. Ackerman, W. L. Smith, A. D. Collard, X. L. Ma, H. E. Revercomb, and R. O. Knuteson, "Cirrus cloud properties derived from high spectral resolution infrared spectrometry during FIRE II. Part II: Aircraft HIS results," *J. Atmos. Sci.*, vol. 52, pp. 4246–4263, 1995.

[53] B. A. Baum, P. F. Soulen, K. I. Strabala, M. D. King, S. A. Ackerman, W. P. Menzel, and P. Yang, "Remote sensing of cloud properties using MODIS airborne simulator imagery during SUCCESS. II. Cloud thermodynamic phase," *J. Geophys. Res.*, vol. 105, pp. 11 781–11 792, 2000.

[54] J. Li, W. P. Menzel, F. Sun, T. J. Schmit, and J. Gurka, "AIRS sub-pixel cloud characterization using MODIS cloud products," *J. Appl. Meteorol.*, vol. 43, pp. 1083–1094, 2004.

Heli Wei received the M.S. degree in atmospheric physics from Anhui Institute of Optics and Fine Mechanics, Chinese Academy of Sciences, Hefei, in 1992.

He is currently a Senior Research Associate with the Department of Atmospheric Sciences, Texas A&M University, College Station. He has been conducting research in the infrared atmospheric radiative transfer, radiative properties of clouds, and remote sensing of cirrus clouds with high-resolution IR spectra.

Ping Yang received the Ph.D. degree in meteorology from University of Utah, Salt Lake City, in 1995.

He is currently an Assistant Professor in the Department of Atmospheric Sciences, Texas A&M University, College Station. After graduation from the University of Utah, he remained with the university for two years, working as a Postdoctoral Researcher. Later, he was an Assistant Research Scientist at University of California, Los Angeles, as well as with the Goddard Earth Sciences and Technologies Center, University of Maryland Baltimore County, Baltimore, as an Associate Research Scientist. His research interests are in remote sensing and radiative transfer. He has been actively conducting research in modeling of optical and radiative properties of clouds and aerosols, in particular, cirrus clouds and their applications to spaceborne and ground-based remote sensing.

Jun Li received the B.S. degree in mathematics from Peking University, Beijing, China, in 1987, and the M.S. and Ph.D. degrees in atmospheric science from the Institute of Atmospheric Physics, Chinese Academy of Sciences, Beijing, in 1990 and 1996, respectively.

In 1997, he jointed the Space Science and Engineering Center (SSEC), University of Wisconsin–Madison, where he was responsible for developing the algorithms to retrieve atmospheric and cloud parameters from the MODIS, NPOESS Airborne Sounder Testbed-Interferometer, and the AIRS measurements. His research interests include deriving atmospheric temperature and moisture profiles, as well as cloud properties from the hyperspectral sounder and the multispectral imager data. He is currently an Associate Scientist with SSEC and the Principal Investigator of future Geostationary Operational Environmental Satellite Hyperspectral Environmental Suite and Advanced Baseline Imager studies at the Cooperative Institute for Meteorological Satellite Studies.

Bryan A. Baum received the Ph.D. degree in atmospheric sciences from the Georgia Institute of Technology, Atlanta, in 1989.

He is currently a Senior Research Scientist with the Radiation and Aerosols Branch, NASA Langley Research Center (LaRC), Hampton, VA, but is stationed at the Cooperative Institute for Meteorological Satellite Studies (CIMSS), University of Wisconsin–Madison. His research activities have focused on satellite, aircraft, and surface-based remote sensing of multilayered cloud properties from multispectral imagery, regional and global cloud-top property retrievals derived from satellite data, global fire and smoke detection, and the effect of clouds and aerosols on the earth's radiation budget.

Hung-Lung Huang was born in Taipei, Taiwan, R.O.C., in 1955. He received the B.S. degree in atmospheric science from National Taiwan University, Taipei, in 1979, and the M.S. and Ph.D. degrees in meteorology from the University of Wisconsin–Madison (UW), in 1986 and 1989, respectively.

From 1979 to 1984, he was a Satellite Meteorologist with the meteorological satellite ground station of the Taiwan Central Weather Bureau. Since 1989, he has been with Cooperative Institute for Meteorological Satellite Studies (CIMSS), UW, as a Research Scientist, conducting remote sensing research in the areas of atmospheric sounding retrieval, information content analysis, satellite and aircraft high spectral resolution sounding instrument data processing, data compression, instrument design and performance analysis, and cloud property characterization. He is currently a Senior Scientist with CIMSS, a GIFTS Mission Scientist, and an Adjunct Professor with the Nanjing Institute of Meteorology, Nanjing, China.

Dr. Huang is a science council member of CIMSS, a council member of the Space Science and Engineering Center of the UW, and is serving a two-year term as the Chair of Committee on Environmental Satellite Data Utilization of the National Research Council of the National Academies.

Steven Platnick received the B.S. degree from Duke University, Durham, NC, and the M.S. degree from the University of California, Berkeley, both in electrical engineering, and the Ph.D. degree in atmospheric sciences from the University of Arizona, Tucson.

He joined the National Aeronautics and Space Administration (NASA) Goddard Space Flight Center (GSFC), Greenbelt, MD, in January 2003, and is currently Deputy Project Scientist of NASA's Aqua satellite. Prior to this appointment, he was a Research Associate Professor in the Joint Center for Earth Systems Technology, University of Maryland Baltimore County, from 1996 to 2002. He has worked in collaboration with NASA GSFC since 1993, and prior to that held engineering positions at Hewlett-Packard Company for six years as well as a National Research Council Resident Research Associate position at NASA Ames Research Center. His research experience includes theoretical and experimental studies of satellite, aircraft, and ground-based cloud remote sensing, including applications to MODIS. He is a member of the MODIS Science Team.

Yongxiang Hu received the Ph.D. degree in atmospheric sciences from the University of Alaska, Fairbanks, in 1994.

He is currently a Senior Research Scientist at the Radiation and Aerosols Branch, NASA Langley Research Center, Hampton, VA. He was a Postdoctoral Researcher at the College of William and Mary and a Research Professor at Hampton University before he joined NASA in 1999. His research interests include radiative transfer, passive and active atmospheric remote sensing, and satellite onboard data analysis.

Larrabee Strow received the B.S. degree from the University of Maryland Baltimore County (UMBC), Baltimore, in 1974, and M.S. and Ph.D. degrees from the University of Maryland, College Park, in 1977 and 1981, respectively, all in physics.

He is currently a Professor with the Department of Physics, UMBC. His research interests include molecular spectroscopy, especially spectral line shapes, and atmospheric remote sensing. He is a member of the AIRS Science Team.